state occurs with a sufficiently low thermal activation barrier that the intermediates not observed at 298 K can be accumulated and characterized at low temperatures.

**Acknowledgment.** We thank the National Science Foundation for support of this research.

**Registry No.** $Et_3SiH$, 617-86-7; $Ph_3SiH$, 789-25-3; $Et_3SiCo(CO)_4$, 14049-72-0; $Et_3SiCo(CO)_3P(OPh)_3$, 75030-69-2; $Et_3SiCo(CO)_3$, 88179-98-0; $Me_3SiCo(CO)_4$, 15693-82-0; $Me_3SiCo(CO)_3$, 88179-99-1; $Ph_3SiCo(CO)_4$, 14095-19-3; $Ph_3SiCo(CO)_3$, 88180-00-1; $(Et_3Si)_2Co(CO)_3H$, 88180-01-2; $(Et_3Si)(Me_3Si)Co(CO)_3H$, 88180-02-3; $(Et_3Si)(Ph_3Si)Co(CO)_3H$, 88180-03-4; $Et_3SiO$, 1631-33-0.

# Single-Crystal Time-of-Flight Neutron Diffraction Structure of Hydrogen *cis*-Diacetyltetracarbonylrhenate, [*cis*-$(OC)_4Re(CH_3CO)_2$]H: A Metallaacetylacetone Molecule

**Arthur J. Schultz,*[1a] K. Srinivasan,[1b] Raymond G. Teller,[1a] Jack M. Williams,[1a] and C. M. Lukehart*[1b]**

*Contribution from the Chemistry Division, Argonne National Laboratory, Argonne, Illinois 60439, and the Department of Chemistry, Vanderbilt University, Nashville, Tennessee 37235.* *Received May 11, 1983*

**Abstract:** A single-crystal time-of-flight neutron diffraction structure of hydrogen *cis*-diacetyltetracarbonylrhenate, [*cis*-$(OC)_4Re(CH_3CO)_2$]H, is reported. This is one of the first successful structure determinations reported by using this technique. The diffraction data were collected at the Argonne Intense Pulsed Neutron Source with the unique time-of-flight single-crystal diffractometer. Complete experimental details are provided. The positions of all hydrogen atoms are determined, and the enolic hydrogen atom is shown to participate in an intramolecular O···H···O hydrogen bond. Although large thermal motion of the enolic hydrogen atom prevents a precise definition of the symmetry of this hydrogen bond, most of the results are consistent with an asymmetric O···H···O bond and a localized $\pi$-electron system within the rhena chelate ring.

In this paper, we report the single-crystal time-of-flight neutron diffraction structure of the rhenaacetylacetone molecule, hydrogen *cis*-diacetyltetracarbonylrhenate, [*cis*-$(OC)_4Re(CH_3CO)_2$]H, **1**.

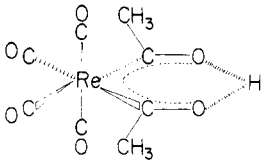

**1**

This investigation was undertaken to unambiguously locate the position of the enolic hydrogen atom and to confirm the presence of O···H···O intramolecular hydrogen bonding. Although the enolic hydrogen atom was not located in a previous X-ray diffraction study of **1**, the molecular structure is consistent with a symmetrical or nearly symmetrical O···H···O enolic hyrogen bond.[2] Furthermore, the low-field $^1H$ NMR resonance at $\delta$ 21.79 (in $CS_2$ solution) for the enolic hydrogen atom of **1** and the O···H···O vibrational stretching frequency of 1658 $cm^{-1}$ (in $C_6H_{12}$ solution) for **1** indicate that extensive O···H···O hydrogen bonding is probably present. Vibrational stretching frequencies near 1650 $cm^{-1}$ for O···H···O bonds have been proposed by others to indicate symmetrical or nearly symmetrical hydrogen bonding.[3]

Because this is one of the first reports[4] of a molecular structure derived from single-crystal time-of-flight neutron diffraction data, we believe a short description of the technique is desirable. The driving force to develop pulsed neutron sources and the instrumentation to utilize them for a wide variety of condensed-matter research[5] is the need for higher neutron flux and shorter data collection times than presently exist at steady-state reactor sources, for which the technical problem of heat removal is the major limiting factor in increasing their flux. Pulsed neutron sources have the advantage that they produce heat for only a small percentage of the time, whereas heat removal is continuous, and therefore the potential exists to produce fluxes orders of magnitude greater than those from reactor sources.[6]

At the Argonne Intense Pulsed Neutron Source (IPNS),[7] neutrons are generated by a pulsed spallation process in which short bursts of high-energy (500-MeV) protons are used to bombard a target of heavy nuclei (e.g., depleted uranium) 30 times per second (see Figure 1). The high-energy neutrons emanating from the target are thermalized by a hydrogen-containing moderator (e.g., polyethylene or liquid methane). Beam lines for each of the IPNS instruments are grouped radially around each of the four moderators. At a distance $l$ from the moderator, the wavelength $\lambda$ of a neutron is determined by the de Broglie equation:

$$\lambda = \frac{h}{mv} = \left(\frac{h}{m}\right)\left(\frac{t}{l}\right)$$

where $h$ is Planck's constant, $m$ is the neutron mass, $v$ is the velocity of the neutron, and $t$ is the time-of-flight for flight path,

(1) (a) Argonne National Laboratory. (b) Vanderbilt University.
(2) Lukehart, C. M.; Zeile, J. V. *J. Am. Chem. Soc.* **1976**, *98*, 2365-2367.
(3) (a) Ratajczak, H.; Orville-Thomas, W. J. *J. Mol. Struct.* **1967**, *1*, 449-461. (b) Joesten, M. D.; Schaad, L. J. In"Hydrogen Bonding"; Marcel Dekker: New York, 1974.
(4) Schultz, A. J.; Teller, R. G.; Beno, M. A.; Williams, J. M.; Brookhart, M.; Lamanna, W; Humphrey, M. B. *Science (Washington D.C.)* **1983**, *220*, 197-199.
(5) For a complete description of pulsed neutron sources and instrumentation see: Windsor, C. G. "Pulsed Neutron Scattering"; Halsted Press: New York, 1981.
(6) Carpenter, J. M. *Nucl. Instrum. Methods* **1977**, *145*, 91-113.
(7) Carpenter, J. M.; Price, D. L.; Swanson, N. J. "IPNS-A National Facility for Condensed Matter Research", Report No. ANL-78-88; Argonne National Laboratory; Argonne, IL, 1978.

0002-7863/84/1506-0999$01.50/0 

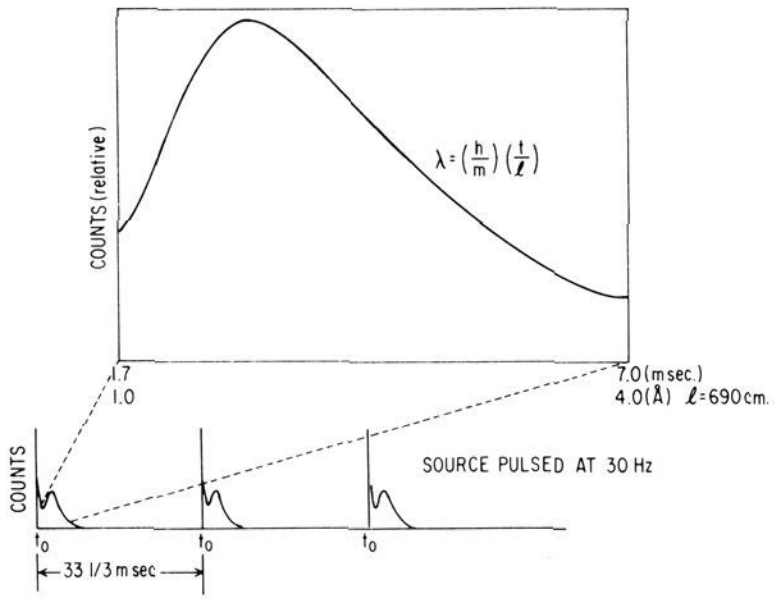


**Figure 1.** At IPNS, neutrons are produced by bombarding a target of depleted uranium with small bursts of protons 30 times per second. The moment when the proton burst hits the target is $t_0$. By use of the de Broglie relationship, the neutron wavelength is related to its time-of-flight for a known flight path $l$ (see also Figure 3). The drawing shows the relative neutron flux vs. wavelength for each pulse.

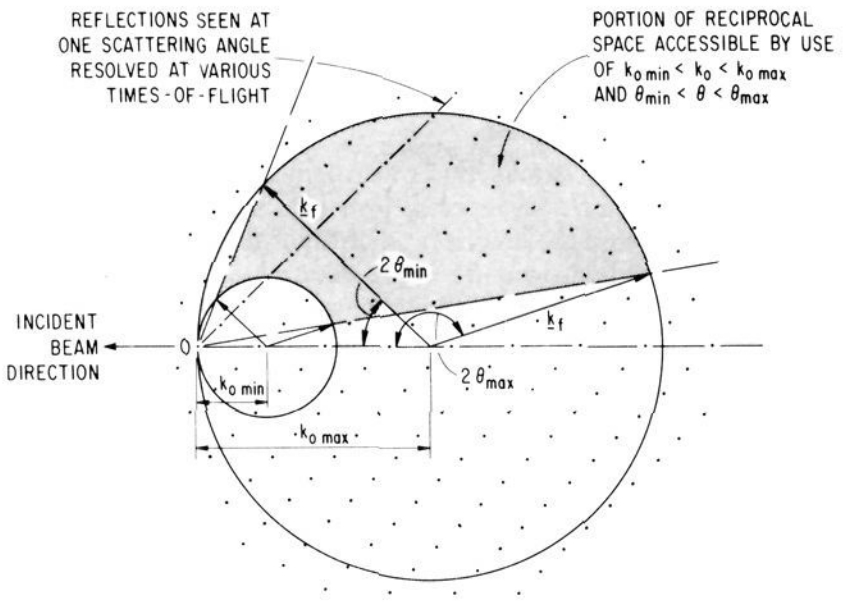


**Figure 2.** Construction in reciprocal space to illustrate the use of multiwavelength radiation in single crystal diffraction. The circles with radii $k_{0max} = 2\pi/\lambda_{min}$ and $k_{0min} = 2\pi/\lambda_{max}$ are drawn through the origin. In two dimensions, all reciprocal lattice points within the shaded area may be sampled by a linear position-sensitive detector spanning $2\theta_{min}$ to $2\theta_{max}$. With a position-sensitive area detector, a three-dimensional portion of reciprocal space may be sampled.

*l.* In a conventional diffraction experiment with monochromatic radiation, the Bragg equation $d = \lambda/(2 \sin \theta)$ is satisfied by varying the $2\theta$ angle. As illustrated in Figure 2 for the multiwavelength case, an entire reciprocal lattice row can be scanned by varying wavelength with a single element detector fixed at the proper angle. With a pulsed neutron source the neutrons are sorted out by velocity, and therefore by wavelength, and the individual Bragg reflections can be resolved by time of flight. Furthermore, Figure 2 shows that for any crystal orientation, possibly hundreds of reflections satisfy the Bragg equation during each pulse, the number depending on unit cell size and wavelength range. In order to exploit this feature, we have developed a single-crystal diffractometer[8] with a large area position-sensitive detector[9] that permits sampling reciprocal space in three dimensions during each pulse (see Figure 3). Without the time of flight, or wavelength resolution, the data would be analogous to a Laue photograph

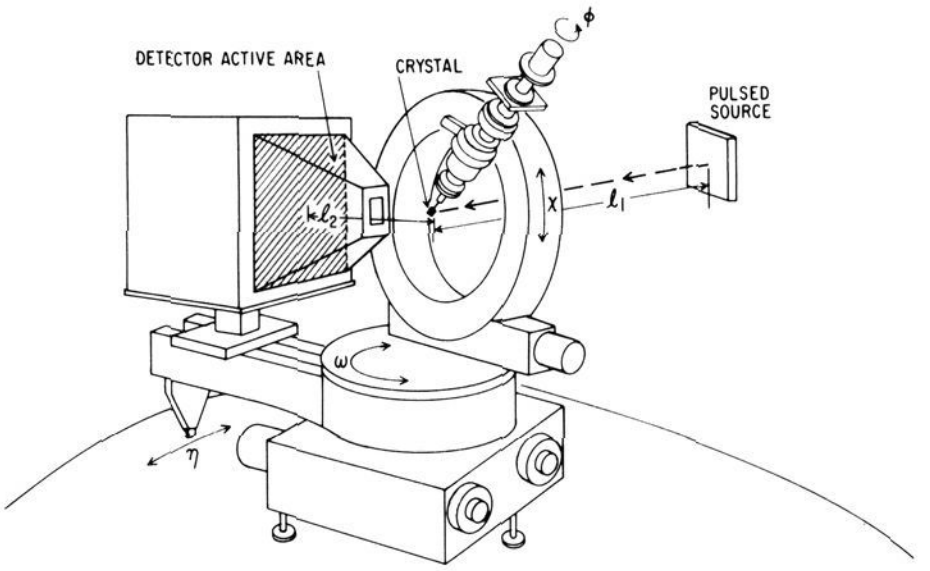


**Figure 3.** A schematic representation of the single-crystal diffractometer at the IPNS. The position-sensitive area (30 × 30 cm) detector is in the shielded enclosure on the detector arm. The angle $\eta$ is the angle of the detector arm with the incident neutron beam. Typical distances for $l_1$ and $l_2$ are 665 and 25 cm, respectively.

obtained with white radiation in which all orders of a $d$-spacing overlap resulting in loss of intensity information.

Some of the features of the single-crystal time-of-flight Laue technique[10,11] with a pulsed spallation neutron source are as follows: (1) Pulsed spallation neutron sources have the potential of producing multiwavelength time-averaged fluxes orders of magnitude greater than the monochromatic flux on sample at high-flux reactor sources. (2) With conventional monochromatic techndiques, only a very small portion of the available neutrons are selected by Bragg scattering from a single crystal. With time-of-flight techniques, nearly all the available neutrons can be utilized. (3) Because a three-dimensional portion of reciprocal space is sampled during each pulse, many Bragg reflections can be measured "simultaneously". Furthermore, it will be easier to characterize diffuse and superlattice scattering in three dimensions. (4) It is not necessary to accurately know the crystal orientation in order to accurately measure the Bragg intensities. (5) While counts are collected in a histogram, both the sample and detector are stationary. (6) It is necessary to accurately measure or calculate the wavelength dependencies of many factors, including the incident spectrum, the detector efficiency, and absorption and extinction corrections.

The first three items in the list can lead to higher overall data rates and the use of generally smaller crystals approaching the size used for conventional X-ray studies. Features 3 and 4 are highly advantageous for studying temperature- (or pressure-) dependent phase transitions and for quickly characterizing the scattering in three dimensions. Feature 6 is probably the major difficulty with the time-of-flight Laue technique, since the precision of the results are limited by the accuracy of determining the incident spectrum and other wavelength-dependent parameters.

## Experimental Section

**Preparation and Crystallization of [*cis*-$(OC)_4Re(CH_3CO)_2$]H.** To a solution of 1.53 g of $CH_3C(O)Re(CO)_5$ in 50 mL of ether at 0 °C was added 2.50 mL of a 1.6 M solution of methyllithium in ether. The reaction solution was stirred at 0 °C for 30 min and then was cooled to −78 °C, and 2.0 mL of a 2.57 M HCl/ether solution was added to the reaction solution. After the reaction solution was stirred for 5 min at −78 °C, it was warmed to 0 °C and was stirred at that temperature for 40 min. The solvent was removed at low pressure, and the reaction residue was extracted with 3 × 25 mL portions of hexane. Filtration of the extraction solutions and subsequent removal of the solvent at low pressure afforded 0.68 g of the crude product. Compound characterization data have been reported previously.[2] Large crystals were obtained by crystallization from ether solution at −15 °C.

(8) Peterson, S. W.; Reis, Jr., A. H.; Schultz, A. J.; Day, P. In "Solid State Chemistry: A Contemporary Overview"; Holt, S. J., Milstein, J. B., Robbins, M., Eds.; American Chemical Society: Washington, DC, 1980; Adv. Chem. Ser. No. 186, pp 75–91.

(9) (a) Strauss, M. G.; Brenner, R.; Lynch, F. J.; Morgan, C. B. *IEEE Trans. Nucl. Sci.* **1981**, NS-28, 800. (b) Schultz, A. J.; Teller, R. G.; Williams, J. M.; Strauss, M. G.; Brenner, R. *Trans. Am. Cryst. Assoc.* **1982**, *18*, 169–179.

(10) Buras, B.; Mikke, K.; Zebech, B.; Lecicjewicz, *J. Phys. Stat. Sol.* **1965**, *11*, 567.

(11) Schultz, A. J.; Teller, R. G.; Peterson, S. W.; Williams, J. M. In "Neutron Scattering-1981", AIP Conference Proceedings No. 89; Faber, Jr., J., Ed.; American Institute of Physics: New York, 1982; p 35–41.

Table I. Data Collection Parameters

| | |
|---|---|
| sample-to-detector distance | 25.5 cm |
| sample-to-moderator distance | 664.7 cm |
| detector angle, $\eta$ | 90.00° |
| $\omega$ angle | 45.00° |
| detector dimensions | 28.0 × 27.5 cm |
| neutron source repetition rate | 30 Hz |
| histogram dimensions | |
| $X,Y$ | 85 × 85 channels |
| $T$ | 116 channels |
| wavelength range | |
| histograms 1-10 | 1.000-3.995 Å |
| histograms 11-23 | 1.400-3.394 Å |
| histogram channel widths | |
| $X,Y$ | 0.33 × 0.32 cm |
| $T$, hists. 1-10 | 45 μs., 0.026 Å |
| $T$, hists. 11-23 | 30 μs., 0.017 Å |

**Instrument Description.** The single-crystal diffractometer (SCD) consists of a Huber orienter, with $\chi$ and $\phi$ motion, on an Electronics & Alloys base for $\omega$ and detector angle motion (see Figure 3). The detector is a unique, position-sensitive $^6$Li-glass scintillation detector[9] with an active area of 30 × 30 cm and a spacial resolution of 3 mm. It was designed and developed at Argonne to provide higher detector efficiency and virtually no parallax relative to the conventional multiwire $^3$He gas proportional counter. Each neutron event is characterized by three digitized coordinates representing position on the detector ($X$ and $Y$) and time-of-flight ($t$). The data are stored in histogram form in 2.5 Mbytes of random access memory (RAM) by a Z8001 microcomputer. A $BF_3$ detector in the direct beam is used to monitor the incident flux. The user controls the instrument through interaction with a PDP 11/34 computer which is linked to three 10-Mbyte disks, a 6250 BPI tape drive, a CRT terminal, a printing terminal, a color CRT screen for graphics displays, and two CAMAC crates with modules for receiving data from the detectors and sending commands to the diffractometer stepping motors.

A schematic representation of the instrument is shown in Figure 3. For a typical experiment, the crystal-to-moderator distance is 664 cm and the crystal-to-detector distance is 26 cm. Thus, a neutron wavelength range of 1.0 to 4.0 Å requires collecting data between 1.7 and 7.0 ms from the beginning of each pulse. With a detector angle $\eta$ of 90°, a nominal $2\theta$ range of 60 to 120° is accessed, which combined with the wavelength range provides a $(\sin\theta)/\lambda$ range of 0.13 to 0.87 Å$^{-1}$.

**Data Collection.** The first step in the data collection procedure is to calculate a table of $\chi$ and $\phi$ setting values that provide coverage of a hemisphere in reciprocal space. It is important to realize that the settings only depend on the instrument parameters (crystal-to-detector distance, detector dimensions, $\eta$) and not on the unit cell or the orientation matrix of the particular crystal, since the individual reflections are not centered in the detector. Therefore, a previous table of settings can be used with any crystal if the instrument parameters are the same. During automatic data collection, the crystal is rotated to one of the $\chi$ and $\phi$ settings and data are accumulated for a preset monitor count. Upon reaching the preset monitor count, the histogram is transferred from the RAM memory to a disk and tape, memory is zeroed, the crystal is rotated to the next set of $\chi$ and $\phi$ angles, and data collection is resumed. Of course, while data are being collected both the crystal and the detector are stationary. The user is able to characterize the crystal in a minimum amount of time by displaying "live" data from the RAM memory or data stored on disk using a variety of graphics programs. Depending on the scattering ability of the crystal and the level of counting statistics desired, the counting time per histogram could typically range from 3 to 12 h.

For this experiment, a crystal of [*cis*-$(OC)_4Re(CH_3CO)_2]H$[12] (**1**) weighing 5 mg with approximate dimensions of 1.0 × 2.0 × 3.5 mm was sealed in a quartz-glass dome on an aluminum pin under a nitrogen atmosphere. The crystal was then mounted in a general orientation on the IPNS SCD, and a total of 23 histograms were obtained at room temperature. The first 10 of these had a wavelength range of 1.0-3.0 Å and the remaining 13 had a wavelength range of 1.4-3.4 Å. We decided to change the wavelength range nearly halfway into the data collection because the high-order data (i.e., short wavelength) were all very weak or unobserved. A summary of the instrument and data collection parameters is presented in Table I.

**Data Analysis.**[11] Most of the data analysis is accomplished with a library of programs[13] on a VAX 11/780 computer linked to the PDP 11/34 front-end computer. Initially, a few histograms are automatically searched for strong Bragg reflections, which are then stored in a file with appropriate positional and wavelength information. A selection of these data are used in an autoindexing program to obtain cell parameters and an orientation matrix. The positions and indices of reflections in each histogram are predicted from the orientation matrix, and the region around the predicted positions are integrated in three dimensions. For the crystal of **1**, the space group is $P2_1/n$, and unit cell parameters of $a$ = 6.258 (3), $b$ = 17.533 (12), $c$ = 10.088 (7) Å, and $\beta$ = 96.02 (5)° were obtained from a least-squares fit of 397 Bragg peaks. Since the dimensions of individual peaks in terms of histogram units are only approximately 5 × 5 × 5 in the detector $X$ and $Y$ and the time (i.e., wavelength) directions, the observed peak position is not well determined and many peaks are included in the least-squares to obtain reasonable standard deviations. The cell parameters obtained from the X-ray study[3] are $a$ = 6.264 (1) Å, $b$ = 17.510 (4) Å, $c$ = 10.036 (6) Å, and $\beta$ = 96.18 (2)°.

The conversion of integrated intensities to structure factor amplitudes is based on the Laue formula:[10,11]

$$I_{hkl} = kT\phi(\lambda)\epsilon(\lambda)A(\lambda)y(\lambda)|F_{hkl}|^2\lambda^4/\sin^2\theta$$

where $k$ is a scale factor, $T$ is the normalized monitor count, $F_{hkl}$ is the structure factor, and $\theta$ is the Bragg angle. The wavelength-dependent factors are the incident flux $\phi(\lambda)$, the detector efficiency $\epsilon(\lambda)$, the absorption correction $A(\lambda)$, and the extinction correction $y(\lambda)$. The incoherent scattering from a vanadium sample is used to provide a normalization factor representing the product of $\phi(\lambda)$ and $\epsilon(\lambda)$ at wavelength $\lambda$.[14] Each Bragg reflection is also corrected for the percent dead time loss at wavelength $\lambda$ based on a random sampling of the dead time during the data collection.[9b]

The absorption correction $A(\lambda)$ was obtained by first calculating the linear absorption coefficients for the crystal at $\lambda$ = 1.0 Å ($\mu$ = 1.13 cm$^{-1}$) and at $\lambda$ = 3.4 Å ($\mu$ = 2.39 cm$^{-1}$). The linear absorption coefficients for wavelengths between the two end points was determined by a simple linear interpolation, which is a reasonable approximation in the absence of nuclear resonances for any of the elements in the crystal. The correction $A(\lambda)$ was then calculated by using an approximated crystal shape of a cylinder with a radius of 0.055 cm.

**Structure Refinement.** The non-hydrogen atomic parameters obtained from the X-ray study[2] were refined with the neutron data by using isotropic thermal parameters to give an $R(F_o)$ factor of 0.26. All seven hydrogen atoms were located in a difference map with phase angles calculated from the non-hydrogen atomic coordinates. In the final stages of refinement, a separate scale factor was included for each histogram with a range of values of 1.64 (4) to 1.96 (5). A secondary extinction correction $y(\lambda)$ based on the Zachariasen formulation[15] was also included, and all atoms were refined with anisotropic thermal parameters. A scaled difference map based on the final parameters was featureless. A summary of the least-squares refinements is given in Table II. Table III

Table II. Least-Squares Refinement[a]

| | |
|---|---|
| number of reflections | |
| all data | 2596 |
| $F^2 > 2\sigma(F^2)$ | 1170 |
| number of parameters varied for data > $2\sigma(F^2)$ | 222 |
| range of scale factors | 1.64 (4)-1.96 (5) |
| extinction parameter, $g$ | 0.17 (2) × 10$^{-4}$ |
| range of ext. corr. $y(\lambda)$ | 1.00-1.27 |
| $R(F)$ | 0.128 |
| $R(F^2)$ | 0.136 |
| $R_w(F^2)$ | 0.110 |
| "goodness-of-fit", $\sigma_1$ | 1.65 |

[a] Based on minimization of $\Sigma w_i|F_o^2 - S^2F_c^2|$, where $S$ is a scale factor and the individual weights $w_i = 1/\sigma^2(F_o^2)$.

(12) For a detailed preparative procedure see: Darst, K. P.; Lukehart, C. M.; Warfield, L. T.; Zeile, J. V. *Inorg. Synth.* **1980**, *20*, 200-204.

(13) Some of the programs used in analyzing the data: ANVLS, least-squares for multiwavelength data, based on the Oak Ridge program ORXFLS3; ANVRED, data reduction including corrections for all wavelength-dependent factors; BLIND, autoindexing for time-of-flight data; HNTINT, Bragg peak integration program; LSQRS, unit cell and orientation matrix least squares; PEKSER, without an orientation matrix, search histogram for peaks, interpolate and integrate; TABLE, calculate a table of diffractometer angle settings with the least overlap. Major contributors to the SCD program library include A. J. Schultz, R. G. Teller, A. H. Reis, Jr., and R. A. Jacobson (Iowa State University) and H. A. Levy (Oak Ridge National Laboratory).

(14) (a) Day, D. H.; Johnson, D. A. G.; Sinclair, R. N. *Nucl. Instrum. Methods* **1969**, *70*, 164-168. (b) Lebech, B.; Mikke, K.; Sledziewska-Blocka, D. *Ibid.* **1970**, *79*, 51-54.

(15) Zachariasen, W. H. *Acta Crystallogr.* **1967**, *23*, 558-564.

Table III. Atomic Positional Parameters (with esd's) for [*cis*-$(OC)_4Re(CH_3CO)_2$]H

| atom | x | y | z |
|---|---|---|---|
| Re | 0.2020 (6) | 0.1261 (4) | 0.7612 (6) |
| O1 | 0.597 (2) | 0.1902 (8) | 0.922 (2) |
| O2 | 0.612 (3) | 0.054 (2) | 0.895 (2) |
| O3 | −0.130 (2) | 0.0083 (9) | 0.625 (2) |
| O4 | 0.048 (2) | 0.1055 (7) | 1.045 (2) |
| O5 | 0.436 (2) | 0.1466 (7) | 0.507 (2) |
| O6 | −0.134 (2) | 0.253 (1) | 0.784 (2) |
| C1 | 0.403 (3) | 0.295 (1) | 0.837 (3) |
| C2 | 0.430 (2) | 0.2099 (6) | 0.8515 (9) |
| C3 | 0.418 (4) | −0.0407 (8) | 0.774 (3) |
| C4 | 0.438 (4) | 0.0420 (6) | 0.818 (1) |
| C5 | −0.003 (2) | 0.516 (7) | 0.677 (1) |
| C6 | 0.0979 (9) | 0.1126 (5) | 0.9378 (9) |
| C7 | 0.345 (2) | 0.4106 (6) | 0.5956 (9) |
| C8 | −0.010 (2) | 0.2079 (7) | 0.7121 (9) |
| H1A | 0.523 (8) | 0.324 (2) | 0.871 (6) |
| H1B | 0.376 (9) | 0.306 (2) | 0.735 (5) |
| H1C | 0.269 (6) | 0.308 (2) | 0.875 (4) |
| H2A | 0.611 (3) | 0.118 (2) | 0.916 (2) |
| H3A | 0.280 (6) | −0.064 (2) | 0.815 (4) |
| H3B | 0.365 (6) | −0.048 (2) | 0.679 (5) |
| H3C | 0.561 (7) | −0.072 (3) | 0.806 (4) |

Table IV. Selected Interatomic Distances (Å) and Angles (deg) with esd's for [*cis*-$(OC)_4Re(CH_3CO)_2$]H

| atoms | distance | atoms | distance |
|---|---|---|---|
| Re-C2 | 2.18 (2) | C3-C4 | 1.52 (2) |
| Re-C4 | 2.13 (2) | C2-O1 | 1.25 (2) |
| Re-C5 | 1.96 (2) | C1-C2 | 1.51 (2) |
| Re-C6 | 1.97 (2) | O1-H2A | 1.26 (4) |
| Re-C7 | 1.99 (1) | O2-H2A | 1.15 (4) |
| Re-C8 | 1.98 (2) | C1-H1A | 0.94 (5) |
| C5-O3 | 1.19 (2) | C1-H1B | 1.03 (5) |
| C6-O4 | 1.16 (2) | C1-H1C | 0.99 (5) |
| C7-O5 | 1.11 (2) | C3-H3A | 1.08 (4) |
| C8-O6 | 1.12 (2) | C3-H3B | 0.98 (5) |
| C4-O2 | 1.28 (2) | C3-H3C | 1.07 (5) |
| **atoms** | **angle** | **atoms** | **angle** |
| C2-Re-C5 | 179.0 (5) | C5-Re-C8 | 89.1 (5) |
| C4-Re-C8 | 177.5 (5) | C3-C4-O2 | 112 (2) |
| C6-Re-C7 | 172.5 (4) | C1-C2-O1 | 114 (2) |
| Re-C2-O1 | 122 (1) | C2-O1-H2A | 108 (2) |
| Re-C2-C1 | 124.5 (9) | C4-O2-H2A | 105 (2) |
| Re-C4-O2 | 125 (2) | O1-H2A-O2 | 172 (2) |
| Re-C4-C3 | 123.2 (9) | C2-C1-H1A | 115 (3) |
| Re-C5-O3 | 178 (2) | C2-C1-H1B | 106 (3) |
| Re-C6-O4 | 176.1 (6) | C2-C1-H1C | 106 (2) |
| Re-C7-O5 | 175.7 (9) | C4-C3-H3A | 107 (3) |
| Re-C8-O6 | 178 (2) | C4-C3-H3B | 115 (3) |
| C2-Re-C4 | 87.1 (4) | C4-C3-H3C | 111 (3) |
| C2-Re-C8 | 90.4 (5) | C4-Re-C5 | 93.4 (5) |

contains the final atomic positional parameters, and Table IV presents selected interatomic distances and angles. In Tables III and IV, numerical values are rounded in the usual fashion, but the values of the esd's are always rounded to the next larger digit. A table of atomic anisotropic thermal parameters and a table of observed and calculated structure factors are included as supplementary material. The large standard deviations in positional coordinates and distances and angles appear to be due to the very large atomic thermal parameters. Similar results for the non-hydrogen atoms were obtained from the X-ray diffraction study.[2]

## Results and Discussion

An ORTEP diagram of complex **1** showing the atomic numbering scheme is shown in Figure 4. The coordination geometry about the Re atom is as expected for a *cis*-$L_2Re(CO)_4$ complex. The principal axial coordination axis defined by the C(6)-Re-C(7) angle of 172.5 (4)° is bent slightly toward the enolate chelate ring. A similar distortion is observed in the X-ray structure where the C(6)-Re-C(7) angle is 170.6 (6)°. The remaining two principal coordination axes of the Re pseudooctahedral complex are more nearly linear having an average C-Re-C angle of 178.3 (5)°. The

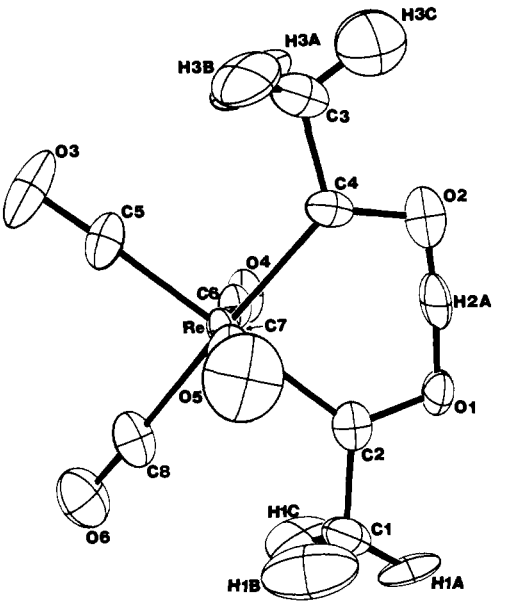


**Figure 4.** An ORTEP diagram of [*cis*-$(OC)_4Re(CH_3CO)_2$]H showing the atomic numbering scheme.

average value of all cis OC-Re-CO angles is 90 (3)°, and the average values of the Re-C and C-O distances are 1.98 (2) and 1.15 (2) Å, respectively. The average value of the Re-C-O angles of the terminal CO ligands is 177 (2)°.

The C(1) and C(3) methyl groups have the expected pyramidal geometry. The C(1)-C(2) and C(3)-C(4) methyl carbon-acyl carbon distances are 1.51 (2) and 1.52 (2) Å, respectively. The average value of the six C-H distances is 1.02 (5) Å, and the average value of the six C-C-H angles is 110 (3)°.

The structural feature of complex **1** of particular interest is the geometry of the rhenaacetylacetonate ring including the enolic O···H···O hydrogen bond. Idealized structural extremes are shown as **2** and **3**. Structure **2** represents a localized $\pi$-electron system

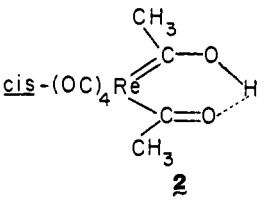


**2**

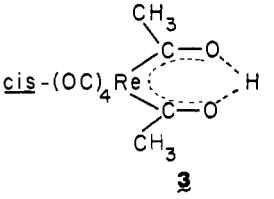


**3**

within the rhena chelate ring and an unsymmetrical O-H···O hydrogen bond, while structure **3** represents a delocalized $\pi$-electron system within the rhena chelate ring and a symmetrical or centered O···H···O hydrogen bond.

A comparison of the rhenaacetylacetonate ring geometry as determined by X-ray and neutron diffraction is shown in **4** and **5**, respectively. The corresponding bond distances and angles

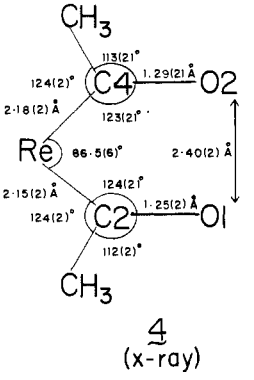


**4**
(x-ray)

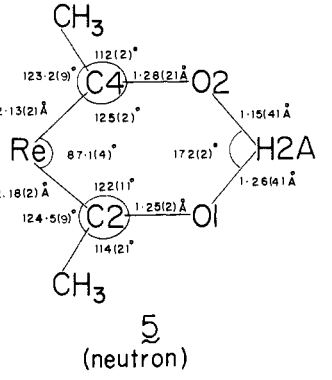


**5**
(neutron)

shown (as determined by each method) are equivalent to within

$\pm 1.5\sigma$. The poorest correspondence, though still within this limit, is the Re-C(4) distance.

A comparison of the intra-chelate ring bond distances of similar type within **5** indicates a slightly unsymmetrical rhenaacetylacetonate ring. The difference between the two Re-C distances, the two C-O distances, and the two O-H(2A) distances is consistent with a slight distortion toward structure **2**. Furthermore, a partial difference Fourier map, phased with all the atoms but with H(2A) excluded from the structure factor calculation, also exhibits an asymmetric O···H···O bond consistent with **5** and **2**. However, it must be noted that structure **5** is symmetrical, as shown in **3** within the $\pm 1.5\sigma$ limit. Also, the numerical asymmetry shown in **4** (as determined by X-ray diffraction) is not consistent with **2** and might indicate that any observed asymmetry in the neutron structure is not significant because of the relatively large standard deviations.

Both structural determinations give an O(1)···O(2) bite distance of 2.40 (2) Å. The corresponding bite distance in tetraacetylethane, which exists as the dienolic tautomer, is 2.42 Å.[16] In one survey of structures containing O-H···O hydrogen bonds, it was concluded that an observed O···O distance of less than 2.47 Å indicates a probable symmetrical hydrogen bond.[17] In the neutron structure **5** reported here, the position of the enolic hydrogen atom, H(2A), is determined. The O(1)-H(2A)-O(2) angle of 172 (2)° indicates a slightly bent hydrogen bond. The two O-H(2A) distances are numerically nonequivalent by 0.11 Å, although this difference is within $\pm 1.5\sigma$ and might not be significant. Large thermal motion, also observed in the X-ray structure, apparently prevents the precise location of the enolic hydrogen atom. Oscillation between two closely spaced enolic hydrogen atom positions, as might be expected if a double-minimum asymmetric hydrogen bond exists,[18] might account for the directional feature of this thermal motion.

A more recent analysis of very short O···H···O hydrogen bonds (defined as having an O···O nonbonding distance in the range of 2.40–2.50 Å) that have been studied by neutron diffraction reveals that centered or symmetric hydrogen bonds and asymmetric hydrogen bonds are observed with nearly equal frequency.[19] Of those bonds previously considered to be symmetric, recent findings indicate that many are actually disordered or asymmetric.[20] These observations further complicate the classification of the O···H···O hydrogen bonding observed in **1** since the very short O(1)···O(2) distance of 2.40 (3) Å does not require that a centered O···H···O hydrogen bond be present. The effectively centered O···H···O hydrogen bond observed in potassium hydrogen chloromaleate reveals O···H distances of 1.199 (5) and 1.206 (5) Å, an O-H-O angle of 175.4 (4)° and an O···O distance of 2.403 (3) Å.[19] Pyridine-2,3-dicarboxylic acid has an asymmetrical O-H···O hydrogen bond having O-H distances of 1.163 (5) and 1.238 (5) Å, an O-H···O angle of 174.4 (4)°, and an O···O distance of 2.398 (3) Å.[21] Relative to these structural extremes, the O(2)-H(2A) and O(1)-H(2A) distances in **5** of 1.15 (4) and 1.26 (4) Å are numerically quite consistent with an asymmetrical O-H···O hydrogen bond. However, the large standard deviations on these distances prevents a conclusive structural definition of the type of hydrogen bonding within the rhenaacetylacetone molecule.[22]

## Conclusion

This paper reports one of the first molecular structure determinations obtained by single-crystal time-of-flight neutron diffraction. The existence of a strong intramolecular O···H···O bond in the rhenaacetylacetone molecule, [*cis*-$(OC)_4Re(CH_3CO)_2H$], is established unambiguously. Although large thermal motion prevents a conclusive definition of the bonding in the rhena chelate ring, the neutron diffraction results appear to be consistent with a localized $\pi$-electron system and an asymmetric O···H···O bond.

**Acknowledgment.** C.M.L. acknowledges support from the National Science Foundation (Grant No. CHE-8106140), the University Research Council of Vanderbilt University, and the Alfred P. Sloan Foundation as a Research Fellow. K.S. thanks the Argonne Universities Association for support of this project. The work at Argonne National Laboratory was supported by the Office of Basic Energy Sciences, Division of Materials Sciences, U.S. Department of Energy, under Contract W-31-109-Eng-38.

**Registry No. 1**, 59299-78-4; $CH_3C(O)Re(CO)_5$, 23319-44-0; methyllithium, 917-54-4.

**Supplementary Material Available:** Tables of structure factors and thermal parameters (7 pages). Ordering information is given on any current masthead page.

(16) Schaefer, J. P.; Wheatley, P. J. *J. Chem. Soc. A* **1966**, 528-532.
(17) Pimentel, G. C.; McClellan, A. L. *Annu. Rev. Phys. Chem.* **1971**, *22*, 347-385.
(18) De La Vega, J. R. *Acc Chem. Res* **1982**, *15*, 185-191.
(19) Olovsson, I.; Jösson, P.-G. In "The Hydrogen Bond. II. Structure and Spectroscopy"; Schuster, P., Zundel, G., Sandorfy, C., Eds.; North-Holland: Amsterdam, 1976; pp 395-456.
(20) Joswig, W.; Fuess, H.; Ferraris, G. *Acta Crystallogr. Sect. B* **1982**, *B38*, 2798-2801.
(21) Kvick, Å.; Koetzle, T. F.; Thomas, R.; Takussagawa, F. *J. Chem. Phys.* **1974**, *60*, 3866-3874.
(22) The X-ray structure of acetylacetone has been reported recently.[23] The acetylacetone molecule exists as the enol tautomer with an asymmetric O-H···O hydrogen bond. The values of the two O-H distances, the O···O nonbonding distance, and the O-H···O angle are 1.03 Å, 1.66 Å, 2.535 Å, and 141°, respectively.
(23) Camerman, A.; Mastropaolo, D.; Camerman, N. *J. Am. Chem. Soc.* **1983**, *105*, 1584-1586.

# Polypeptide Complexes of Silver(III)

**Louis J. Kirschenbaum* and James D. Rush**

*Contribution from the Department of Chemistry, University of Rhode Island, Kingston, Rhode Island 02881.* *Received August 1, 1983*

**Abstract:** Trivalent silver complexes of triglycine ($G_3$) and tetraglycine ($G_4$) have been prepared by direct reaction of the ligand with $Ag(OH)_4^-$ in aqueous alkali media. The multistep formation reaction of $Ag^{III}G_4$ is accompanied by a silver ion catalyzed path and a competing redox path. These complexes have characteristic spectra and, except for the method of preparation, are strikingly similar to the analogous Cu(III) system studied by Margerum and co-workers. The region of maximum stability ($k_d \sim 7 \times 10^{-3}$ s$^{-1}$ for $Ag^{III}G_4$) is at pH 5-10. The p$K_a$ for the interconversion of $Ag^{III}(H_{-3}G_4)^-$ and $Ag^{III}(H_{-4}G_4)^{2-}$ is about 12.5. Above pH 10 both species decompose mainly by a path involving abstraction of a methylenic proton by $OH^-$ followed by reduction of the metal to $Ag^I$. The net activation energy for $Ag^{III}G_4$ decomposition is about 16 kcal/mol. $Ag^{III}G_3$ is considerably less stable than the tetraglycine complex at lower pH.

Peptide complexes of trivalent copper and nickel have been studied extensively by Margerum and co-workers.[1-7] The tetraglycine complex, $Cu^{III}G_4$,[8] has significant stability in aqueous solution and decomposes by one-electron processes that are both

0002-7863/84/1506-1003$01.50/0 